

Discovery of a High Affinity and Selective Pyridine Analog as a Potential Positron Emission Tomography Imaging Agent for Cannabinoid Type 2 Receptor

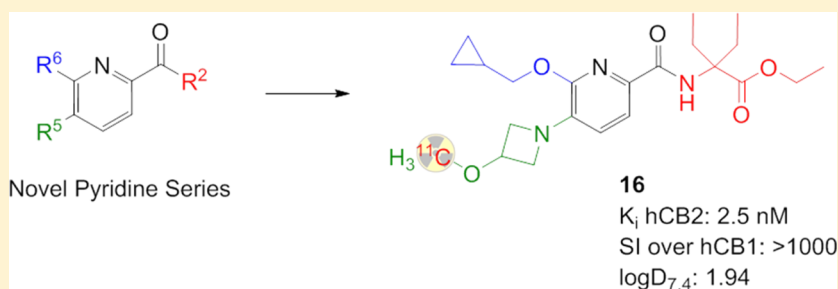
Roger Slavik,[†] Uwe Grether,^{*,‡} Adrienne Müller Herde,[†] Luca Gobbi,[‡] Jürgen Fingerle,[‡] Christoph Ullmer,[‡] Stefanie D. Krämer,[†] Roger Schibli,^{†,§} Linjing Mu,^{†,§} and Simon M. Ametamey^{*,†}

[†]Center for Radiopharmaceutical Sciences ETH, PSI and USZ, Institute of Pharmaceutical Sciences, ETH Zurich, Vladimir-Prelog-Weg 4, CH-8093 Zurich, Switzerland

[‡]Roche Pharmaceutical Research and Early Development, Roche Innovation Center Basel, F. Hoffmann-La Roche Ltd., Grenzacherstrasse 124, 4070 Basel, Switzerland

[§]Department of Nuclear Medicine, University Hospital Zurich, CH-8091 Zurich, Switzerland

S Supporting Information



ABSTRACT: As part of our efforts to develop CB2 PET imaging agents, we investigated 2,5,6-substituted pyridines as a novel class of potential CB2 PET ligands. A total of 21 novel compounds were designed, synthesized, and evaluated for their potency and binding properties toward human and rodent CB1 and CB2. The most promising ligand **6a** was radiolabeled with carbon-11 to yield **16** ($[^{11}\text{C}]\text{RSR-056}$). Specific binding of **16** to CB2-positive spleen tissue of rats and mice was demonstrated by in vitro autoradiography and verified in vivo in PET and biodistribution experiments. Furthermore, **16** was evaluated in a lipopolysaccharid (LPS) induced murine model of neuroinflammation. Brain radioactivity was strikingly higher in the LPS-treated mice than the control mice. Compound **16** is a promising radiotracer for imaging CB2 in rodents. It might serve as a tool for the investigation of CB2 receptor expression levels in healthy tissues and different neuroinflammatory disorders in humans.

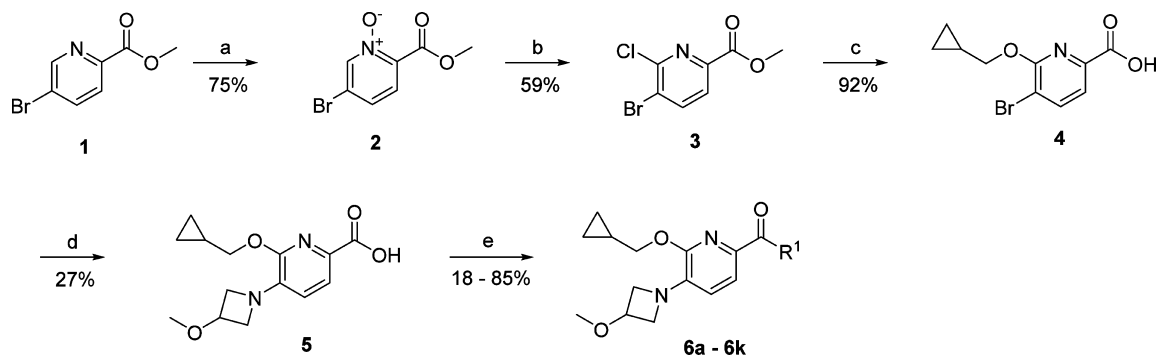
INTRODUCTION

The endocannabinoid system (ES) is a rather complex and tightly regulated signaling system and a key player in several physiological and pathological mechanisms.¹ It has prohomeostatic effects on cannabinoid receptor activation, exerting a general protective function. This system was discovered in the early 90s through investigations on potential targets for cannabidiol (CBD) and Δ^9 -tetrahydrocannabinol (THC), the two pharmacologically most active ingredients of *Cannabis sativa* L.^{2,3} Besides several putative cannabinoid receptors such as GPR55,⁴ GPR119,⁵ GPR18⁶ and TRPV1,⁷ two main subtypes of cannabinoid receptors are known, designated as CB1 and CB2. Both belong to the class A G-protein-coupled receptor family (GPCR) containing seven transmembrane spanning domains. CB1 is highly expressed in the central nervous system (CNS) with highest density in cerebellum, hippocampus, and cortex.⁸ CB2 on the other hand is mainly expressed on cells related to the immune system⁹ but also present in the CNS; however, its expression level is very low.^{10–12} It plays an important (yet not fully understood) role

in neuroinflammatory diseases and is therefore a very promising target for therapeutic approaches as well as for PET imaging in Parkinson's and Alzheimer disease, multiple sclerosis (MS), and amyotrophic lateral sclerosis (ALS).^{13–16}

Several CB2 PET ligands from a diverse class of compounds including quinolines,^{17,18} thiazoles,¹⁹ indoles,^{20,21} oxadiazoles,²² triazines,²³ and bis-sulfones²⁴ have been reported, but to date no optimal ligand exists for the imaging of CB2 in human subjects. As part of our efforts to develop a PET radioligand targeting CB2, we have prepared and evaluated the in vitro binding profiles of a series of 2,5,6-substituted pyridines. The most promising compound **6a** was labeled with carbon-11 to obtain ethyl 2-(6-(cyclopropylmethoxy)-5-(3-(methoxy- ^{11}C)-azetidin-1-yl)picolinamido)-2-ethylbutanoate ($[^{11}\text{C}]\text{RSR056}$) and evaluated in rats and in a murine model of neuroinflammation.

Received: February 17, 2015

Scheme 1. Synthesis of 5-Methoxyazetidinyridine Derivatives 6a–k^a

^aReagents and conditions: (a) *m*-CPBA, CH₂Cl₂, reflux, 20 h; (b) POCl₃, 95 °C, 1 h; (c) (1) cyclopropylmethanol, NaH, 95 °C, 3 h; (2) H₂O, rt, 10 min; (d) methoxyazetidine, Cs₂CO₃, [Pd₂(dba)₃], BINAP, 110 °C, toluene, 16 h; (e) DIPEA, DMTMM, H₂NR¹, rt, CH₂Cl₂, 16 h.

Table 1. Lipophilicity (log *D*), Binding Affinity (*K*_i), and Potency (EC₅₀) Values of Compounds 6a–k^g

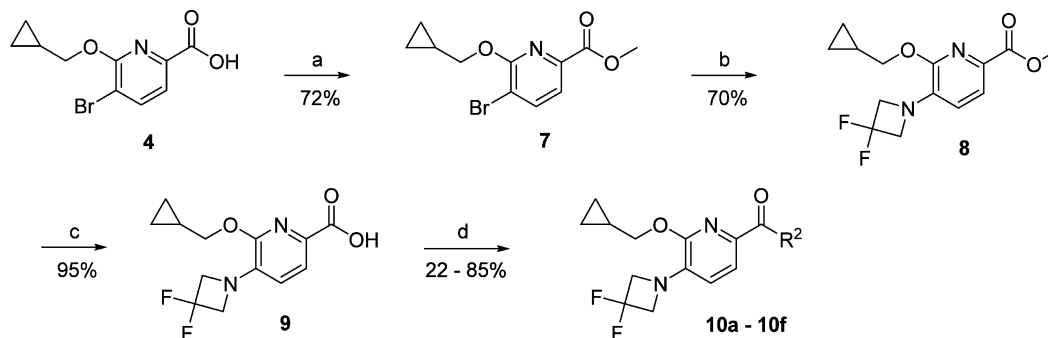
Compd	clogP	PSA [Å ²]	R ²	logD	<i>K</i> _i [μM]		EC ₅₀ [μM]	
					hCB2	mCB2	hCB2	hCB1
6a	4.59	74.37		1.94 [*]	0.0025 ^a	0.0018 ^b	0.0044	>10
6b	3.21	76.84		3.18	0.1698	0.0604	0.047	>10
6c	3.46	76.24		3.43	0.9023 ^c	0.4211 ^c	0.2809	>10
6d	3.69	76.31		3.67	2.0648 ^d	5.261 ^d	0.4443	>10
6e	3.73	69.04		3.25	0.0183 ^c	0.0069 ^c	0.0044	>10
6f	1.71	101.33		1.7	1.0173	3.1135	0.0668	>10
6g	2.91	98.25		nd	>10	2.2779	0.1548	>10
6h	3.68	88.65		nd	0.4659 ^c	0.5040 ^d	1.8054 ^d	>10
6i	3.85	72.44		nd	2.8674	2.226	1.2914	>10
6k	2.68	89.01		3.37	nd ^f	nd	4.0075	>10

^a*n* = 6. ^b*n* = 8. ^c*n* = 3. ^d*n* = 2. ^e*n* = 4. ^fnd = not determined. ^gThe clogP and polar surface area (PSA) are calculated values. If not stated otherwise, values represent data from a single experiment in triplicate. The asterisk (*) indicates log *D* was determined with shake-flask method using radiolabeled compound.

RESULTS

Chemistry. Commercially available methyl-5-bromopyridin-2-carboxylate **1** was treated with *m*-chloroperoxybenzoic acid to afford *N*-oxide **2** in 75% yield (Scheme 1). Reaction of the *N*-oxide with POCl₃ yielded chlorinated compound **3** in 59% yield via an addition–elimination reaction. Treatment with the sodium salt of cyclopropylmethanol and subsequent hydrolysis in a one

pot procedure afforded 5-bromo-6-(cyclopropylmethoxy)pyridin-2-carboxylic acid **4** in 92% excellent yield. Compound **4** was converted in a Buchwald–Hartwig amination with 3-methoxyazetidine to yield the desired key intermediate **5**, which was coupled to appropriate amine building blocks using DMTMM to produce the target compounds **6a–k** (Table 1) in 18–85% yield.

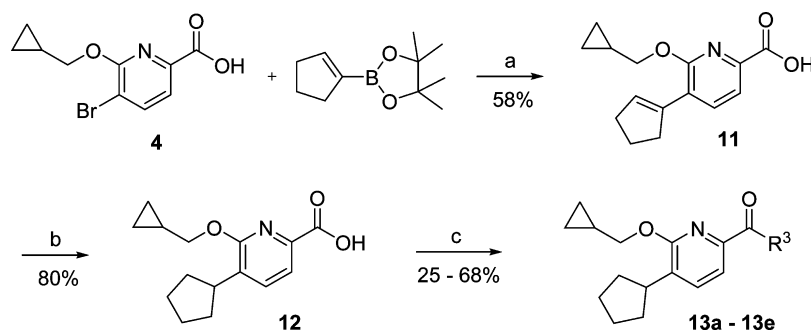
Scheme 2. Synthesis of 5-Difluoroazetidinyrpyridine Derivatives 10a–f^a

^aReagents and conditions: (a) Na₂CO₃, CH₃I, DMF, rt, 16 h; (b) difluoroazetidine HCl, Cs₂CO₃, [Pd₂(dba)₃], BINAP, 70 °C, dioxane, 16 h; (c) LiOH, THF/H₂O, rt, 3 h; (d) DIPEA, DMTMM, H₂NR², rt, CH₂Cl₂, 16 h.

Table 2. Lipophilicity (logD), binding affinity (K_i) and potency (EC₅₀) values of compounds 10a–f^a

Compd	clogP	PSA [Å ²]	R ²	logD	K _i [μM]		EC ₅₀ [μM]	
					hCB2	mCB2	hCB2	hCB1
10a	4.17	68.63		3.76	0.1794	0.2447	0.0043	>10
10b	4.42	67.54		nd	0.7739 ^c	0.4026 ^c	0.027	>10
10c	3.28	90.94		nd	>10	>10	0.3961	>10
10d	4.65	79.92		nd	3.0341	1.0472	2.8897	>10
10e	4.58	80.03		nd	3.9583	>10	>10	>10
10f	3.19	80.03		nd	>10	>10	>10	>10

^aSuperscript c in the table indicates $n = 3$.

Scheme 3. Synthesis of 5-Cyclopentylpyridine Derivatives 13a–e^a

^aReagents and conditions: (a) [Pd(dppf)Cl₂], Na₂CO₃, DMF, 100 °C, 16 h; (b) Pd/C, H₂, EtOH, rt, 4 h; (c) DIPEA, DMTMM, H₂NR³, CH₂Cl₂, rt, 16 h.

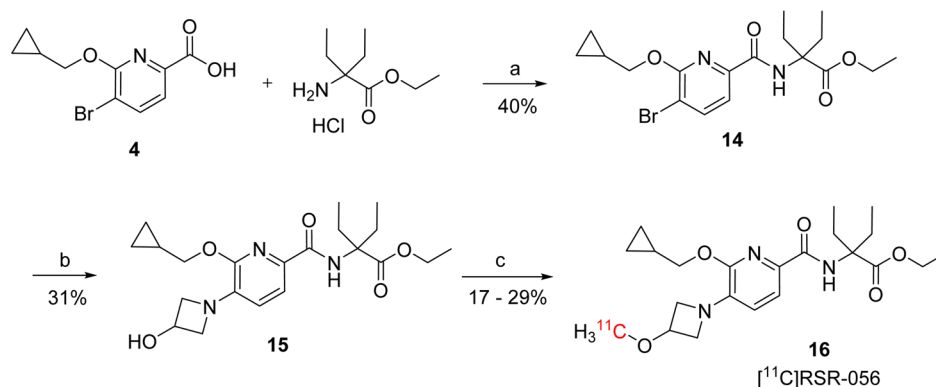
As part of our systematic structure–activity relationship investigation, we replaced the 3-methoxyazetidinyrpyridine substituent in position 5 of the pyridine with difluoroazetidine, applying the reaction sequence described in Scheme 1. Scheme 2 illustrates the synthetic pathway leading to 5-difluoroazetidinyrpyridine

derivatives 10a–f starting from picolinic acid 4. Esterification of the carboxylic functionality was accomplished by reacting the sodium salt of picolinic acid 4 with methyl iodide at room temperature. Methyl ester 7 was reacted with difluoroazetidine using Buchwald–Hartwig reaction conditions to give com-

Table 3. Lipophilicity (log *D*), Binding Affinity (K_i), and Potency (EC_{50}) Values of Compounds 13a–e^a

Compd	clogP	PSA [Å ²]	R ²	logD	K_i [μM]		EC_{50} [μM]	
					hCB2	mCB2	hCB2	hCB1
13a	5.76	58.91		nd	0.0162	0.0385	0.0029	>10
13b	4.06	82.52		nd	0.3519	0.0697	0.0096	0.9482
13c	3.86	78.21		nd	0.2936 ^d	0.0127 ^d	0.1746	>10
13d	4.25	77.91		nd	0.2639 ^d	0.0117 ^d	0.1756	>10
13e	4.85	73.12		nd	0.4161	0.4034	2.7579	>10

^aSuperscript d in the table indicates $n = 2$.

Scheme 4. Synthesis of Precursor 15 and Carbon-11 Labeling of 16^a

^aReagents and conditions: (a) DIPEA, HBTU, DMF, rt, 16 h; (b) 3-methoxyazetidine, Cs₂CO₃, [Pd₂(OAc)₂], toluene, 110 °C, 16 h; (c) [11C]CH₃I, NaH, DMF, 90 °C, 3 min.

compound 8, which was hydrolyzed under basic conditions to provide carboxylic acid 9. Coupling with the appropriate amines afforded target compounds 10a–f (Table 2) in chemical yields ranging from 22% to 85%.

In a further effort, we replaced the azetidine moiety with a cyclopentyl group as outlined in Scheme 3. A palladium catalyzed Suzuki cross-coupling of compound 4 afforded the cyclopentenyl intermediate 11, which underwent reduction with hydrogen using 10% palladium on carbon to afford cyclopentyl analog 12. Coupling of 12 using similar conditions as described in Scheme 1 or Scheme 2 gave the target compounds 13a–e (Table 3) in 25–68% yield.

In Vitro Pharmacology. The selectivity and functional activity of the synthesized compounds toward human CB1 and CB2 were determined in a cAMP assay according to Ullmer et al.²⁵ Binding affinity was determined in a competitive binding assay with membranes prepared from cells expressing human or mouse CB2 receptors (PerkinElmer). EC_{50} or K_i values were calculated from a single experiment using triplicates of 10 different concentrations of compound.

The 5-methoxyazetidine substituted derivatives 6a–k exhibited EC_{50} values in the range of 4 nM to 4 μM (Table 1). The most potent compounds in this series were 6a and 6e,

which both displayed 4.4 nM affinity toward hCB2. The selectivity profile of hCB2 over hCB1 for these compounds was high and greater than 1000. The binding affinities (K_i values) of compound 6a to mouse and human CB2 were also high and comparable to the EC_{50} value obtained using hCB2. The replacement of the ethyl ester group in 6a with the *N*-methyl group as in compound 6b or *N*-fluoroalkyl as in compounds 6c and 6d led to a several-fold decrease in potency. A fluoroazetidine moiety as in derivative 6e exhibited nanomolar activity but was also shown to be a substrate for P-glycoprotein (data not shown). Introducing an oxetane moiety to reduce lipophilicity as in compound 6f showed a promising effect in the cAMP assay with an EC_{50} value of 67 nM, but this value did not correlate with high binding affinity.

Compounds of the 5-difluoroazetidine series shown in Table 2 exhibited EC_{50} values of 4 nM to 2.9 μM. Two compounds, 10e and 10f, from this series of compounds were nonbinders. The *N*-methylamide analogue 10a exhibited the highest potency with an EC_{50} value of 4.3 nM, which, however, did not translate in high binding affinity to human or mouse CB2. Compared to the 5-methoxyazetidine series, the *N*-fluoroethyl side chain as in compound 10b resulted in a more than 10-fold increase in potency ($EC_{50} = 27$ nM). Oxadiazole compounds

10c–e were among the weakest CB2 ligands tested in this work.

Table 3 summarizes the results obtained for the 5-substituted cyclopentylpyridine derivatives. The potency of compounds 13a–e on hCB2 was in the range of 2.9 nM to 2.8 μ M with compound 13a as the most potent derivative. The carboxylate ester 13b was highly active on hCB2, exhibiting an EC₅₀ value of 9.6 nM, but showed insufficient selectivity of \sim 100-fold over CB1. Introducing small PEG chains as in isoxazol derivatives 13c and 13d resulted in rather low potency with EC₅₀ values of 175 and 176 nM, respectively.

From the series of compounds tested in vitro, compound 6a from the group of 5-methoxyazetidine substituted pyridine derivatives emerged as the most promising candidate and was therefore selected for further evaluation. Important properties that prompted our decision included high binding affinity toward mouse and human CB2 receptor, high selectivity, low polar surface area, stability in buffer, optimal membrane permeability, non-Pgp substrate, and amenability to radiolabeling with carbon-11.

Synthesis of Precursor and Radiolabeling. In Scheme 4 are depicted the synthesis of the desmethyl precursor 15 using Buchwald–Hartwig amination reaction and the radiosynthesis of [¹¹C]RSR-056 (16). Compound 16 was successfully obtained by reacting the sodium salt of 15 with [¹¹C]MeI in >99% radiochemical purity after HPLC purification. Total synthesis time was \sim 35 min from end of bombardment, and total radioactivity obtained was 4.1 ± 0.7 GBq ($n = 22$). Specific activity at end of synthesis amounted to 194 ± 139 GBq/ μ mol.

In Vitro Characterization of 16. Radiolabeled compound 16 was stable in formulated solution over a time course of 2 h. Lipophilicity (log *D*) of 16 was measured in *n*-octanol/phosphate buffer at pH 7.4 using the shake-flask method. The log *D*_{7.4} value obtained was 1.94 ± 0.08 ($n = 5$), which is within the optimal range of brain penetrating compounds of 1–3.²⁶ The stability of 16 in mouse, rat, and human plasma was measured at 37 °C over a time course of 40 min. In rat and mouse plasma, 86% and 84%, respectively, of intact compound was found. No radioactive degradation products of 16 were observed in human plasma after 40 min. Sections of rat and mouse spleen, an organ with high basal CB2 levels,²⁷ were used for the in vitro autoradiography experiments (Figure 1). Compound 16 markedly bound to spleen tissue, and the binding was reduced by co-incubation with 5 μ M CB2-selective compound 1-(2,3-dichlorobenzoyl)-5-methoxy-2-methyl-3-[2-

(4-morpholinyl)ethyl]-1*H*-indole (GW405833, 17),²⁸ indicating specific binding of 16 to CB2.

In Vivo Characterization of 16 in Healthy Rats. Baseline dynamic PET acquisitions were performed with 16 in rats for 60 min. For displacement studies, 17 (1.5 mg/kg) was injected iv 10 min after injection of the radiotracer. Figure 2A shows coronal PET images of the spleen (white arrow) under baseline and displacement conditions. The spleen could be clearly detected during the first 10 min after injection of 16. Radioactivity cleared after 10 min under baseline conditions and more rapidly after displacement with 17. Figure 2B shows the corresponding time–activity curves (TACs) comparing tracer uptake in spleen and background (muscle) under baseline and displacement conditions. Spleen-TACs reached background levels 15 min after injection of displacer. Tracer clearance from spleen was considerably enhanced after injection of 17, indicating competitive displacement of 16 from CB2 binding sites.

To confirm the PET data, biodistribution of 16 was studied in rats 15 min after iv injection of 6–10 MBq (0.03–0.05 nmol) of the tracer under baseline and blocking conditions (Figure 3). For blocking conditions, 1.5 mg/kg 17 was injected iv 1 min prior to tracer (9–10 MBq, 0.04–0.05 nmol, $n = 3$) administration. High uptake of 16 was observed in the spleen, which was reduced by 79% upon blockade. Radioactivity uptake in the brain was rather low, which is in agreement with low CB2 levels under normal conditions. Highest activity was detected in the small intestine and liver as is expected of a rather lipophilic xenobiotic.

The metabolic stability of 16 was studied in a male Wistar rat ($n = 1$). Blood samples were collected at different time points and after 20 min, brain and urine were collected and analyzed by radio-TLC. In brain tissue, no activity was detected after 20 min. The percentage of intact parent tracer in plasma decreased with time to 51% after 5 min, 37% after 10 min, and 21% after 20 min. Radioactivity in urine was fully attributed to hydrophilic radiometabolites.

In Vivo Characterization of 16 in a Neuroinflammatory Mouse Model. To prove uptake of 16 in brain with elevated CB2 levels, we used a lipopolysaccharide (LPS) mouse model of neuroinflammation described by Qin et al.²⁹ but with a dose of 10 mg/kg LPS based on mRNA and autoradiographic studies performed in our laboratories.³⁰ Mice were injected with 10 mg/kg LPS 5 days prior to brain PET scan. Increased accumulation of 16 was found in the whole brain after LPS treatment compared to vehicle group (0 mg/kg LPS) (Figure 4). Additionally, 2 mg/kg 17 was subcutaneously injected 30 min prior PET acquisition. Accumulation of 16 in the brain was remarkably reduced under these blockade conditions but did not reach baseline levels.

DISCUSSION

CB2 plays a crucial (yet not fully understood) role in neuroinflammatory diseases. To gain deeper insight into the pathophysiology on a molecular basis, a specific CB2 PET tracer would be very useful.

Considering the structure–activity relationship results described in the patent literature,³¹ we designed a series of 2,5,6-substituted pyridines as novel potential CB2 PET tracers based on the fact that various sets of 2-, 5-, and 6-substituted pyridines show high binding affinity and selectivity toward CB2. At position 2 of the pyridine ring, carboxamides are well tolerated, whereas position 5 tolerates smaller lipophilic

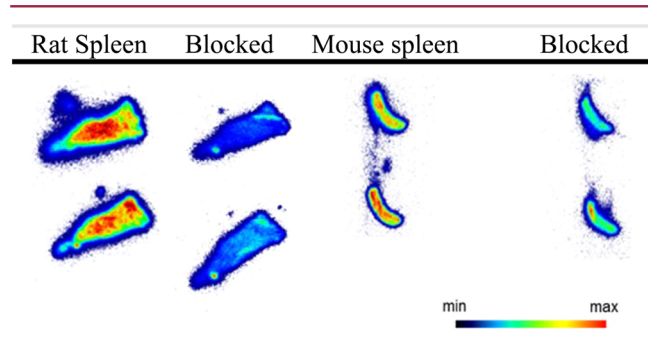


Figure 1. Rat and mouse spleen autoradiograms after incubation with 16 (0.2 nM) under baseline and blocking (5 μ M 17) conditions.

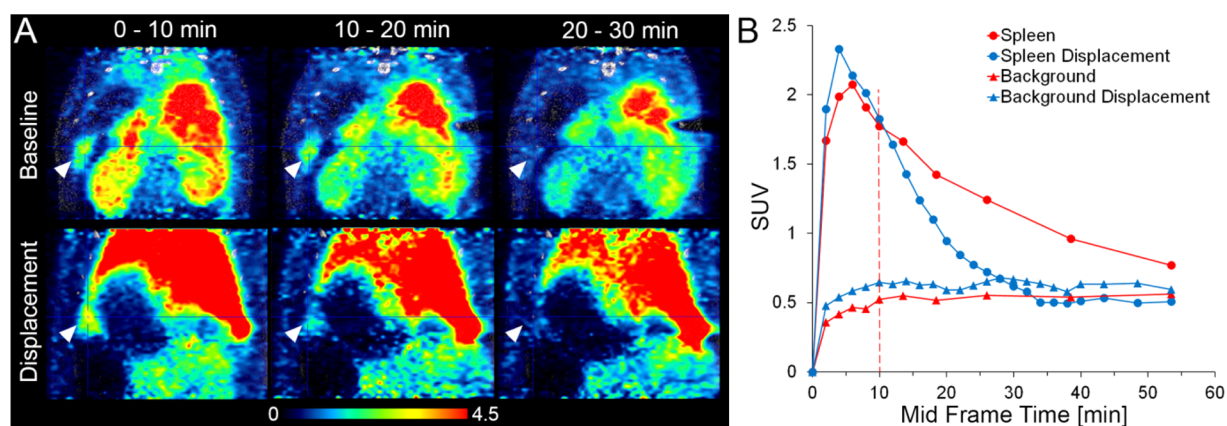


Figure 2. In vivo uptake of **16** in rat spleen under baseline and displacement (1.5 mg/kg **17** injected 10 min after radiotracer) conditions. (A) Coronal **16** PET/CT images. PET images were averaged to three 10 min sequences. White arrow indicates spleen. Color bar indicates standardized uptake value (detected kBq/cm³ normalized by injected kBq/g body weight, SUV). (B) **16**-TACs of spleen and background tissue (muscle) from baseline and displacement experiments.

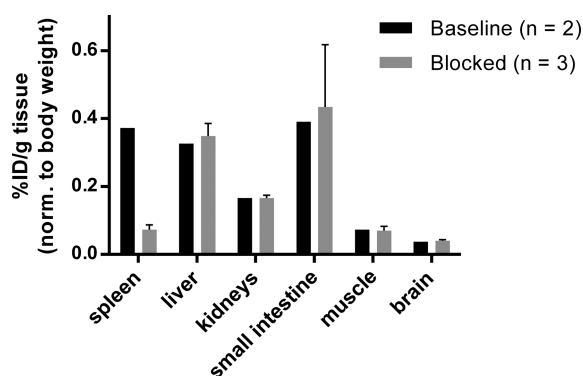


Figure 3. Biodistribution study in rats. Animals were sacrificed 15 min after injection of **16**: 6–10 MBq (0.03–0.05 nmol, $n = 2$) for baseline and 9–10 MBq (0.04–0.05 nmol, $n = 3$) for blocking conditions.

substituents such as halogens, methyl, cyclic alkyls, pyrrolidine, or substituted azetidines. Cycloalkyl or cycloalkylalkoxy are particularly useful moieties in position 6. On the basis of these facts, three carboxylic acid key intermediates **5**, **9**, and **12** were synthesized. The synthetic pathways toward the three intermediates were similar. The cyclopropylmethoxy substituent in position 6 of the pyridine ring was introduced by chlorination followed by S_NAr etherification. In a second step, palladium catalyzed Suzuki cross-coupling or Buchwald–Hartwig amination reactions were used to install the substituents at position 5. Cyclopropyl derivative **12** required an additional reduction step under hydrogen atmosphere. The final products were obtained by amide coupling reactions. Because of the rather low yields of compound **5** in the first Buchwald reaction (Scheme 1), the carboxylic acid functionality in compound **4** was protected as methyl ester to afford compound **7** (Scheme 2), which was used for the amination reaction. The yield for the amination of **7** was significantly higher with 70%. The overall yields for the key intermediate compounds **5**, **9**, and **12** were 11%, 20%, and 19%, respectively. Target compounds **6a–k**, **10a–f**, and **13a–e** were synthesized in 18–85% yields and screened in competition binding assays with hCB1 and hCB2.

With the exception of compound **13b**, all the newly synthesized compounds exhibited high selectivity over CB1. In general, potency and binding affinity to hCB2 were not

always correlated well, and species differences between mouse and human were observed in some examples. Carboxylic acid building block **5** was shown to be particularly useful, as its derivatives possess high binding affinity to CB2 and high selectivity over CB1. Combination with a fluoroazetidine amine building block afforded compound **6e** with excellent single digit nanomolar potency on hCB2 and optimal lipophilicity but suffered from interactions with both human and mouse P-gp efflux protein. From all the novel compounds evaluated, **6a** exhibited the most promising profile and was therefore selected for radiolabeling with carbon-11.

Radiolabeling of **16** was accomplished starting from hydroxyl precursor **15** using [¹¹C]methyl iodide. High chemical purity of the precursor compound was essential for reliable and high radiochemical yields of the radiolabeled product. The binding of **16** was further evaluated in CB2-positive spleen tissues in vitro and in vivo. Blocking and displacement experiments with the CB2-selective agonist **17** successfully demonstrated the specificity of **16** binding to CB2.

Brain radioactivity was strikingly higher in the LPS-treated mice than the control mice and was highest in an LPS-treated mouse (data not shown) that died during the scan, possibly because of the induced neuroinflammation. The increased uptake in the neuroinflammation model may result from elevated CB2 in the inflamed brain or from an increased tracer influx into the brain due to the disruption of the blood–brain barrier under neuroinflammation³² or from a combination of both. As blood–brain barrier disruption is a common observation in neuroinflammation, tightly linked to the inflammatory processes, an ideal PET tracer for neuroinflammation should be insensitive to the integrity of the blood–brain barrier. This is best achieved with a tracer with maximal extraction at the blood–brain barrier, i.e., with a K_1 equal to the cerebral plasma flow. Brain accumulation is in this case dependent on cerebral blood flow but will not be increased by blood–brain barrier disruption. We are currently investigating the kinetics of our CB2-targeting tracers regarding these characteristics.

17 may not be the ideal blocker for the PET experiments, as it not only blocks tracer binding to the receptor but also affects inflammatory processes by its function as a CB2 agonist. In addition, we cannot exclude that under the applied protocol, CB2 levels were not fully occupied by **17**. One hour after

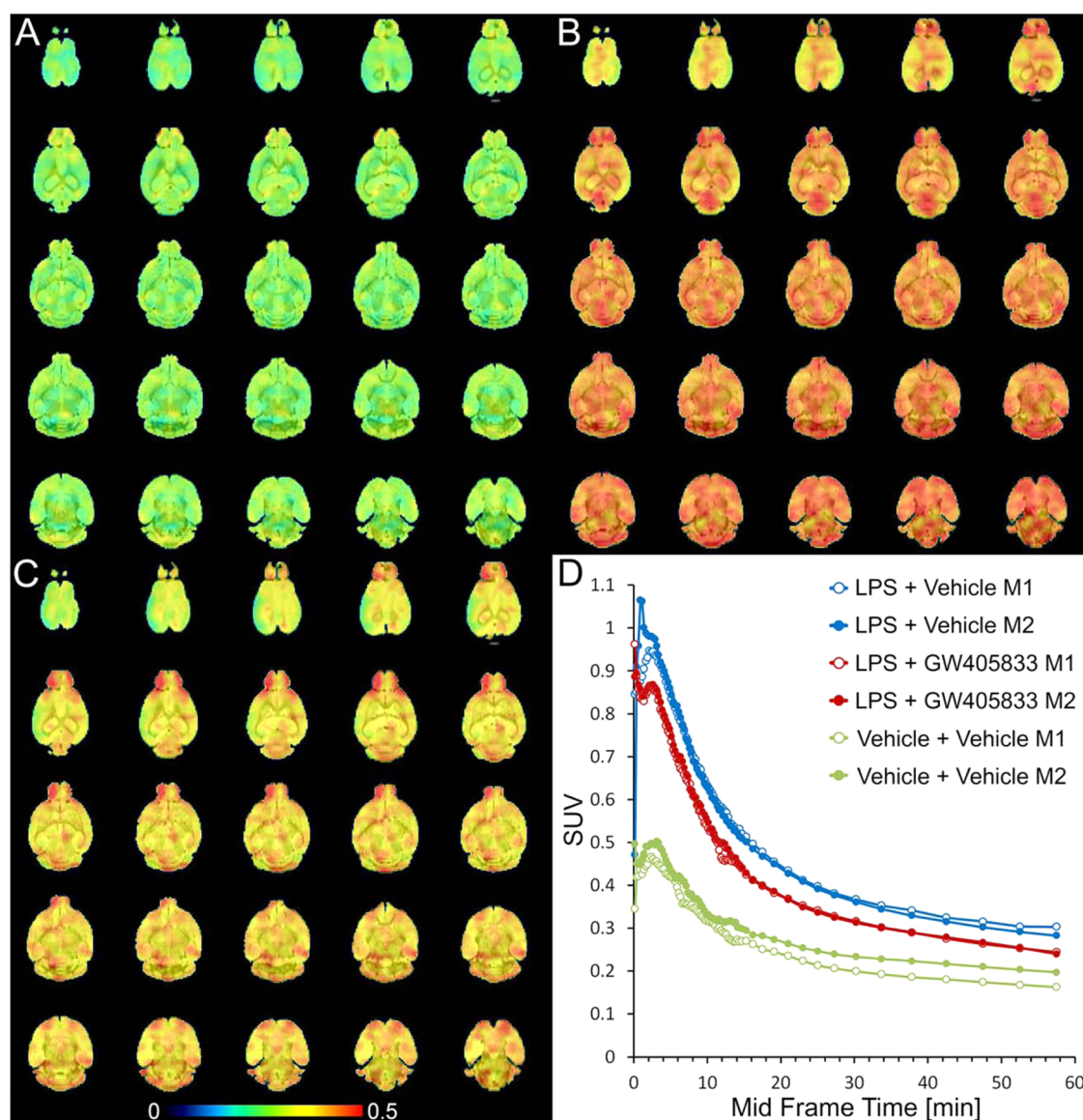


Figure 4. Brain uptake of **16** in LPS mouse model of neuroinflammation. (A–C) Coronal brain PET slices (colored, averaged 0.5–60 min pi) superimposed on an MRI T2 template (gray). (A) Vehicle + vehicle. (B) 10 mg/kg LPS + vehicle. (C) 10 mg/kg LPS + 2 mg/kg **17**. (D) Time-activity curves of the whole brain at the three depicted conditions ($M = \text{mouse}$, $n = 2$).

intraperitoneal injection, levels in rat brain were about 5-fold higher than in plasma.³³ Extrapolating from the plasma levels of the same study, this would result in a brain concentration of $>0.1 \mu\text{M}$ 1 h after intraperitoneal injection. This concentration should be high enough for blockade despite the possibly lower affinity of **17** compared to **16** (K_i values of 3.9,³³ 12,²⁸ or 35 nM²¹ to hCB2 compared to 2.5 nM for **16** and a 150-fold selectivity over hCB1). It should be mentioned here, however, that the affinity of **17** to murine CB2 is not known and remains to be tested.

CONCLUSIONS

We have successfully designed and synthesized a series of 2,5,6-substituted pyridines as CB2 ligands with high selectivity over human CB1. For the most promising compound **6a**, a robust radiosynthesis was established to afford **16** in high yields of 3.0–4.9 GBq, high specific activity of $194 \pm 139 \text{ GBq}/\mu\text{mol}$, and excellent chemical and radiochemical purity of $>99\%$. Specific binding to CB2-positive tissue was demonstrated in

vitro using rodent spleen sections. In vivo studies with PET and biodistribution studies confirmed also the specificity of **16** to spleen tissue. To which extent binding to CB2 and disruption of blood–brain barrier are involved in **16** accumulation in experimental neuroinflammation remains to be elucidated.

In summary, the novel carbon-11 labeled 2,5,6-substituted pyridine derivative **16** is a promising radiotracer for imaging CB2 in rodents and might serve as a tool for the investigation of CB2 receptor levels in healthy tissues and different brain disorders in humans.

EXPERIMENTAL SECTION

General. All reagents and solvents were purchased from Sigma-Aldrich Chemie GmbH (Germany), Merck (Germany), Acros Organics (Belgium), ABCR GmbH (Germany), or Fluka (Switzerland). Purity of synthesized compounds was greater than 95% as determined by analytical HPLC or LC–MS. ¹H spectra were obtained on a Bruker Avance FT-NMR spectrometer. Chemical shifts are given in δ units, in ppm relative to tetramethylsilane (TMS) (0 ppm). Multiplicities in the ¹H NMR spectra are described as s = singlet, d =

6-(Cyclopropylmethoxy)-N-(3-((2-fluoroethyl)carbamoyl)pentan-3-yl)-5-(3-methoxyazetidin-1-yl)picolinamide (6c). Purification: heptane/EtOAc (2:1). Yield: 54% as white powder. ^1H NMR (300 MHz, CDCl_3) δ 8.45 (s, 1H), 7.84 (d, $J = 8.0$ Hz, 1H), 7.64 (d, $J = 8.0$ Hz, 1H), 6.75–6.88 (m, 1H), 4.35–4.46 (m, 3H), 4.26–4.34 (m, 4H), 4.22 (d, $J = 7.3$ Hz, 2H), 4.05 (s, 3H), 3.84–3.92 (m, 3H), 3.55–3.73 (m, 2H), 2.35–2.53 (m, 2H), 1.77–1.92 (m, 2H), 1.11–1.18 (m, 1H), 0.85 (t, $J = 7.4$ Hz, 6H), 0.49–0.59 (m, 2H), 0.34–0.43 (m, 2H). LC–MS (ESI): 435.3 [$\text{M} - \text{H}^-$].

6-(Cyclopropylmethoxy)-N-(3-((3-fluoropropyl)carbamoyl)pentan-3-yl)-5-(3-methoxyazetidin-1-yl)picolinamide (6d). Purification: $\text{CH}_2\text{Cl}_2/\text{MeOH}$ (140:1). Yield: 54% as white powder. ^1H NMR (300 MHz, CDCl_3) δ 8.44 (s, 1H), 7.64 (d, $J = 7.9$ Hz, 1H), 6.74 (t, $J = 5.4$ Hz, 1H), 6.58 (d, $J = 7.9$ Hz, 1H), 4.61 (t, $J = 5.7$ Hz, 1H), 4.46 (t, $J = 5.7$ Hz, 1H), 4.25–4.35 (m, 3H), 4.22 (d, $J = 7.1$ Hz, 2H), 3.83–3.92 (m, 2H), 3.47 (q, $J = 6.5$ Hz, 2H), 3.34 (s, 3H), 2.34–2.49 (m, 2H), 1.74–2.04 (m, 4H), 1.28–1.33 (m, 1H), 0.84 (t, $J = 7.4$ Hz, 6H), 0.57–0.65 (m, 2H), 0.35–0.42 (m, 2H). LC–MS (ESI): 451.5 [MH^+].

6-(Cyclopropylmethoxy)-N-(3-(3-fluoroazetidine-1-carbonyl)pentan-3-yl)-5-(3-methoxyazetidin-1-yl)picolinamide (6e). Purification: heptane/EtOAc (2:1). Yield: 18% as white powder. ^1H NMR (300 MHz, CDCl_3) δ 8.66 (s, 1H), 7.63 (d, $J = 7.9$ Hz, 1H), 6.58 (d, $J = 7.9$ Hz, 1H), 5.35–5.24 (m, 1H), 4.18–4.55 (m, 9H), 3.81–3.92 (m, 2H), 3.34 (s, 3H), 2.52–2.66 (m, 2H), 1.68–1.80 (m, 2H), 1.29–1.32 (m, 1H), 0.86–0.79 (m, 6H), 0.56–0.64 (m, 2H), 0.36–0.44 (m, 2H). LC–MS (ESI): 449.3 [MH^+].

N-(3-(2-Amino-2-oxoethyl)oxetan-3-yl)-6-(cyclopropylmethoxy)-5-(3-methoxyazetidin-1-yl)picolinamide (6f). Purification: $\text{CH}_2\text{Cl}_2/\text{MeOH}$ (20:1). Yield: 85% as white powder. ^1H NMR (300 MHz, CDCl_3): δ 8.17 (s, 1H), 7.57 (d, $J = 8.0$ Hz, 1H), 6.54 (d, $J = 8.0$ Hz, 1H), 5.84 (br s, 1H), 5.41 (br s, 1H), 4.88 (d, $J = 7.1$ Hz, 2H), 4.75 (d, $J = 7.1$ Hz, 2H), 4.34–4.25 (m, 3H), 4.15 (d, $J = 7.3$ Hz, 2H), 3.93–3.84 (m, 2H), 3.34 (s, 3H), 3.21 (s, 2H), 1.34–1.20 (m, 1H), 0.65–0.58 (m, 2H), 0.41–0.34 (m, 2H). LC–MS (ESI): 391.2 [MH^+].

6-(Cyclopropylmethoxy)-N-(3-(1-hydroxy-2-methylpropan-2-yl)isoxazol-5-yl)-5-(3-methoxyazetidin-1-yl)picolinamide (6g). Purification: heptane/EtOAc (2:1). Yield: 76% as white solid. ^1H NMR (300 MHz, CDCl_3): δ 7.60 (d, $J = 7.1$ Hz, 1H), 6.47 (d, $J = 8.1$ Hz, 1H), 5.20 (s, 1H), 4.36–4.29 (m, 5H), 4.28 (s, 2H), 4.25–4.20 (m, 2H), 3.99–3.87 (m, 2H), 3.34 (s, 3H), 1.39 (s, 6H), 1.31–1.27 (m, 1H), 0.62–0.54 (m, 2H), 0.38–0.32 (m, 2H). LC–MS (ESI): 417.7 [MH^+].

6-(Cyclopropylmethoxy)-N-(1-(5-(4-fluorophenyl)-1,3,4-oxadiazol-2-yl)-2-methylpropan-2-yl)-5-(3-methoxyazetidin-1-yl)picolinamide (6h). Purification: heptane/EtOAc (1:1). Yield: 62% as a colorless oil. ^1H NMR (300 MHz, CDCl_3): δ 7.79–7.74 (m, 2H), 7.71 (d, $J = 7.9$ Hz, 1H), 7.59 (s, 1H), 7.09–1.02 (m, 2H), 6.61 (d, $J = 7.9$ Hz, 1H), 4.35–4.26 (m, 3H), 3.99 (d, $J = 7.1$ Hz, 2H), 3.87–3.84 (m, 2H), 3.58 (s, 2H), 3.35 (s, 3H), 1.58 (s, 6H), 1.19–1.11 (m, 1H), 0.56–0.50 (m, 2H), 0.29–0.24 (m, 2H). LC–MS (ESI): 496.7 [MH^+].

6-(Cyclopropylmethoxy)-N-((1-hydroxycyclohexyl)methyl)-5-(3-methoxyazetidin-1-yl)picolinamide (6i). Purification: heptane/EtOAc (2:1 to 1:1). Yield: 65% as a colorless oil. ^1H NMR (300 MHz, CDCl_3): δ 7.86 (t, $J = 6.2$ Hz, 1H), 7.68 (d, $J = 7.9$ Hz, 1H), 6.58 (d, $J = 7.9$ Hz, 1H), 4.34–4.25 (m, 3H), 4.14 (d, $J = 7.1$ Hz, 2H), 3.92–3.83 (m, 2H), 3.46 (d, $J = 6.2$ Hz, 2H), 3.35 (s, 3H), 2.62 (s, 1H), 1.67–1.42 (m, 10H), 1.34–1.29 (m, 1H), 0.66–0.56 (m, 2H), 0.39–0.32 (m, 2H). LC–MS (ESI): 390.7 [MH^+].

N-(1-(5-Cyclobutyl-1,3,4-oxadiazol-2-yl)-2-methylpropan-2-yl)-6-(cyclopropylmethoxy)-5-(3-methoxyazetidin-1-yl)picolinamide (6k). Purification: heptane/EtOAc (1:1). Yield: 38% as white solid. ^1H NMR (300 MHz, CDCl_3): δ 7.67 (d, $J = 8.0$ Hz, 1H), 7.61 (s, 1H), 6.59 (d, $J = 8.0$ Hz, 1H), 4.34–4.25 (m, 3H), 4.10 (d, $J = 7.3$ Hz, 2H), 3.88–3.81 (m, 2H), 3.60 (quin, $J = 8.3$ Hz, 1H), 3.46 (s, 2H), 3.34 (s, 3H), 2.31–2.12 (m, 4H), 2.07–1.93 (m, 1H), 1.92–1.77 (m, 1H), 1.55 (s, 6H), 0.91–0.81 (m, 1H), 0.65–0.57 (m, 2H), 0.39–0.32 (m, 2H). LC–MS (ESI): 456.7 [MH^+].

6-(Cyclopropylmethoxy)-5-(3,3-difluoroazetidin-1-yl)-N-(3-(methylcarbamoyl)pentan-3-yl)picolinamide (10a). Purification: heptane/EtOAc (2:1). Yield: 82% as colorless oil. ^1H NMR (300 MHz, CDCl_3): δ 8.61 (s, 1H), 7.67 (d, $J = 7.8$ Hz, 1H), 6.65 (d, $J = 7.8$ Hz, 1H), 6.35–6.24 (m, 1H), 4.39 (t, $J = 12.0$ Hz, 4H), 4.26 (d, $J = 7.3$ Hz, 2H), 2.89 (d, $J = 4.8$ Hz, 3H), 2.59–2.45 (m, 2H), 1.84–1.70 (m, 2H), 1.38–1.21 (m, 2H), 0.83 (t, $J = 7.4$ Hz, 6H), 0.67–0.60 (m, 2H), 0.43–0.37 (m, 2H). LC–MS (ESI): 432.5 [MNa^+].

6-(Cyclopropylmethoxy)-5-(3,3-difluoroazetidin-1-yl)-N-(3-((2-fluoroethyl)carbamoyl)pentan-3-yl)picolinamide (10b). Purification: heptane/EtOAc (2:1). Yield: 22% as a white solid. ^1H NMR (300 MHz, CDCl_3): δ 8.55 (s, 1H), 7.68 (d, $J = 7.9$ Hz, 1H), 6.57–6.68 (m, 2H), 4.60 (t, $J = 4.8$ Hz, 1H), 4.32–4.49 (m, 5H), 4.25 (d, $J = 7.3$ Hz, 2H), 3.66–3.73 (m, 1H), 3.57–3.65 (m, 1H), 2.46–2.60 (m, 2H), 1.73–1.88 (m, 2H), 1.27–1.34 (m, 1H), 0.84 (t, $J = 7.5$ Hz, 6H), 0.59–0.68 (m, 2H), 0.34–0.47 (m, 2H). LC–MS (ESI): 443.4 [MH^+].

6-(Cyclopropylmethoxy)-5-(3,3-difluoroazetidin-1-yl)-N-(2-(5-(pyridin-3-yl)-1,3,4-oxadiazol-2-yl)propan-2-yl)picolinamide (10c). Purification: heptane/EtOAc (2:1). Yield: 85% as a white solid. ^1H NMR (300 MHz, CDCl_3): δ 9.22 (s, 1H), 8.75 (d, $J = 3.6$ Hz, 1H), 8.33 (dt, $J_1 = 1.9$, $J_2 = 8.1$ Hz, 1H), 8.16 (s, 1H), 7.64 (d, $J = 7.8$ Hz, 1H), 7.43 (dd, $J_1 = 5.1$, $J_2 = 7.8$ Hz, 1H), 6.63 (d, $J = 7.8$ Hz, 1H), 4.40 (t, $J = 11.9$ Hz, 4H), 4.24 (d, $J = 7.3$ Hz, 2H), 1.96 (s, 6H), 1.36–1.29 (m, 1H), 0.72–0.65 (m, 2H), 0.45–0.37 (m, 2H). MS (ESI): 470.5 [M^+].

6-(Cyclopropylmethoxy)-5-(3,3-difluoroazetidin-1-yl)-N-(1-(5-(4-fluorophenyl)-1,3,4-oxadiazol-2-yl)-2-methylpropan-2-yl)picolinamide (10d). Purification: heptane/EtOAc (4:1 to 1:1). Yield: 53% as a colorless oil. ^1H NMR (300 MHz, CDCl_3): δ 7.83–7.79 (m, 2H), 7.73 (d, $J = 7.9$ Hz, 1H), 7.65 (s, 1H), 7.10–7.05 (m, 2H), 6.66 (d, $J = 7.9$ Hz, 1H), 4.37 (t, $J = 4.4$ Hz, 4H), 4.04 (d, $J = 7.3$ Hz, 2H), 3.56 (s, 2H), 1.60 (s, 3H), 1.21–1.13 (m, 1H), 0.61–0.54 (m, 2H), 0.32–0.27 (m, 2H). LC–MS (ESI): 502.6 [MH^+].

6-(Cyclopropylmethoxy)-5-(3,3-difluoroazetidin-1-yl)-N-(2-(5-phenyl-1,3,4-oxadiazol-2-yl)propan-2-yl)picolinamide (10e). Purification: heptane/EtOAc (4:1). Yield: 66% as a colorless oil. ^1H NMR (300 MHz, CDCl_3): δ 8.29 (s, 1H), 8.03 (dd, $J_1 = 1.7$, $J_2 = 7.8$ Hz, 2H), 7.66 (d, $J = 7.8$ Hz, 1H), 7.58–7.41 (m, 3H), 6.63 (d, $J = 7.8$ Hz, 1H), 4.40 (t, $J = 12.0$ Hz, 4H), 4.25 (d, $J = 7.3$ Hz, 2H), 1.96 (s, 6H), 1.36–1.29 (m, 1H), 0.72–0.63 (m, 2H), 0.48–0.36 (m, 2H). LC–MS (ESI): 470.6 [MH^+].

N-(2-(5-Cyclopropyl-1,3,4-oxadiazol-2-yl)propan-2-yl)-6-(cyclopropylmethoxy)-5-(3,3-difluoroazetidin-1-yl)picolinamide (10f). Purification: heptane/EtOAc (1:1 to 1:2). Yield: 60% as a white solid. ^1H NMR (300 MHz, CDCl_3): δ 7.82 (s, 1H), 7.70 (d, $J = 7.9$ Hz, 1H), 6.62 (d, $J = 7.9$ Hz, 1H), 4.40 (t, $J = 11.9$ Hz, 4H), 4.15 (d, $J = 7.3$ Hz, 2H), 1.69 (s, 6H), 1.52–1.38 (m, 1H), 1.34–1.28 (m, 1H), 1.06–0.99 (m, 2H), 0.85–0.77 (m, 2H), 0.70–0.62 (m, 2H), 0.41–0.34 (m, 2H). MS (ESI): 434.5 [MH^+].

Ethyl 2-(5-Cyclopentyl-6-(cyclopropylmethoxy)picolinamido)-2-ethylbutanoate (13a). Purification: heptane/EtOAc (4:1 to 2:1). Yield: 68% as a white solid. ^1H NMR (300 MHz, CDCl_3): δ 8.87 (s, 1H), 7.66 (d, $J = 7.5$ Hz, 1H), 7.56 (d, $J = 7.5$ Hz, 1H), 4.34–4.25 (m, 4H), 3.30–3.19 (m, 1H), 2.69–2.55 (m, 2H), 2.12–2.00 (m, 2H), 1.96–1.56 (m, 8H), 1.36–1.31 (m, 4H), 0.78 (t, $J = 7.5$ Hz, 6H), 0.66–0.55 (m, 2H), 0.46–0.39 (m, 2H). MS (ESI): 402.6 [M^+].

2-(5-Aminoisoxazol-3-yl)-2-methylpropyl-5-cyclopentyl-6-cyclopropylmethoxypicolinate (13b). Purification: heptane/EtOAc (4:1). Yield: 67% as a white solid. ^1H NMR (300 MHz, CDCl_3): δ 7.63–7.56 (m, 1H), 7.54–7.48 (m, 1H), 5.21 (s, 1H), 4.32 (s, 4H), 4.27 (d, $J = 7.1$ Hz, 2H), 3.31–3.18 (m, 1H), 2.14–1.97 (m, 2H), 1.84–1.75 (m, 2H), 1.75–1.66 (m, 2H), 1.65–1.56 (m, 2H), 1.41 (s, 6H), 1.35–1.29 (m, 1H), 0.62–0.54 (m, 2H), 0.40–0.34 (m, 2H). LC–MS (ESI): 400.7 [MH^+].

5-Cyclopentyl-6-(cyclopropylmethoxy)-N-(3-(1-(2-methoxyethoxy)-2-methylpropan-2-yl)isoxazol-5-yl)picolinamide (13c). Purification: heptane/EtOAc (2:1). Yield: 26% as a colorless oil. ^1H NMR (300 MHz, CDCl_3): δ 10.19 (s, 1H); 7.79 (d, $J = 7.4$ Hz, 1H), 7.64 (d, $J = 7.4$ Hz, 1H), 6.49 (s, 1H), 4.24 (d, $J = 6.9$ Hz, 2H),

3.62–3.51 (m, 6H), 3.37 (s, 3H), 3.32–3.25 (m, 1H), 2.14–2.04 (m, 2H), 1.84–1.57 (m, 6H), 1.48–1.41 (m, 1H), 1.36 (s, 6H), 0.69–0.63 (m, 2H), 0.44–0.39 (m, 2H). LC–MS (ESI): 458.7 [MH⁺].

5-Cyclopentyl-6-(cyclopropylmethoxy)-N-(3-(1-(2-ethoxyethoxy)-2-methylpropan-2-yl)isoxazol-5-yl)picolinamide (13d).

Purification: heptane/EtOAc (20:1 to 9:1). Yield: 25% as a colorless oil. ¹H NMR (300 MHz, CDCl₃): δ 10.20 (s, 1H), 7.79 (d, *J* = 7.5 Hz, 1H), 7.64 (d, *J* = 7.5 Hz, 1H), 6.49 (s, 1H), 4.24 (d, *J* = 6.9 Hz, 2H), 3.63–3.48 (m, 8H), 3.35–3.22 (m, 1H), 2.15–2.01 (m, 2H), 1.88–1.59 (m, 6H), 1.36 (s, 6H), 1.19 (t, *J* = 7.0 Hz, 3H), 0.70–0.62 (m, 2H), 0.45–0.38 (m, 2H). LC–MS (ESI): 472.8 [MH⁺].

5-Cyclopentyl-6-(cyclopropylmethoxy)-N-(1-(5-(4-fluorophenyl)-1,3,4-oxadiazol-2-yl)-2-methylpropan-2-yl)picolinamide (13e).

Purification: heptane/EtOAc (4:1 to 2:1). Yield: 49% as a white solid. ¹H NMR (300 MHz, CDCl₃): δ 7.85 (s, 1H), 7.80–7.76 (m, 2H), 7.73 (d, *J* = 7.5 Hz, 1H), 7.60 (d, *J* = 7.5 Hz, 1H), 7.07–7.00 (m, 2H), 4.04 (d, *J* = 7.0 Hz, 2H), 3.58 (s, 2H), 3.27–3.16 (m, 1H), 2.09–2.00 (m, 2H), 1.88–1.64 (m, 6H), 1.60 (s, 6H), 1.20–1.14 (m, 1H), 0.55–0.49 (m, 2H), 0.30–0.25 (m, 2H). LC–MS (ESI): 479.7 [MH⁺].

Ethyl 2-(5-Bromo-6-(cyclopropylmethoxy)picolinamido)-2-ethylbutanoate (14). To a solution of **4** (423 mg, 1.56 mmol) in DMF (10 mL) was added DIPEA (0.731 mL, 4.19 mmol), and the mixture is stirred at rt for 30 min. HBTU (1043 mg, 2.75 mmol) was added portionwise, and after 1 h, ethyl 2-amino-2-ethylbutanoate hydrochloride (234 mg, 1.196 mmol) was added. The mixture is stirred for 16 h, diluted with EtOAc (100 mL), and washed with 0.2 M HCl (3 × 15 mL), water (15 mL), and then brine (20 mL). Solvents were evaporated under reduced pressure and the residue was purified over silica gel using hexane/EtOAc (10:1) and additionally via preparative HPLC using isocratic MeCN/0.1% TFA in water (70:30) to give compound **14** in a yield of 40% as a yellow oil. ¹H NMR (300 MHz, CDCl₃): δ 8.85 (s, 1H), 7.95 (d, *J* = 7.8 Hz, 1H), 7.59 (d, *J* = 7.8 Hz, 1H), 4.37 (d, *J* = 7.0 Hz, 2H), 4.30 (q, *J* = 7.1 Hz, 2H), 2.61–2.55 (m, 2H), 1.94–1.85 (m, 2H), 1.42–1.31 (m, 4H), 0.77 (t, *J* = 7.4 Hz, 6H), 0.66–0.61 (m, 2H), 0.49–0.45 (m, 2H). MS (ESI): 414.4 [MH⁺].

Precursor Compound Ethyl 2-(6-(Cyclopropylmethoxy)-5-(3-hydroxyazetidin-1-yl)picolinamido)-2-ethylbutanoate (15). In a 2.5 mL vial were combined **14** (170 mg, 0.411 mmol), azetidin-3-ol HCl (54.1 mg, 0.494 mmol), diacetoxypalladium (9.23 mg, 0.041 mmol), and Cs₂CO₃ (335 mg, 1.028 mmol) in toluene (2.2 mL). The reaction mixture was vigorously stirred at 110 °C for 16 h. The reaction mixture was filtered on a pad of Celite, and the filtrate was diluted with EtOAc (25 mL). The resulting solution was washed with 0.2 M HCl (3 × 10 mL). Solvents were dried over MgSO₄ and removed under reduced pressure. The crude material was prepurified over silica gel using hexane/EtOAc (4:1 to 2:1) and finally via preparative HPLC using ACN/0.1% TFA in water (50:50) to give **15** in a yield of 31% as a yellowish oil. ¹H NMR (300 MHz, CDCl₃): δ 8.64 (s, 1H), 7.61 (d, *J* = 7.9 Hz, 1H), 6.57 (d, *J* = 7.9 Hz, 1H), 4.78–4.69 (m, 1H), 4.40–4.30 (m, 2H), 4.30–4.21 (m, 4H), 3.83 (m, 2H), 2.72–2.45 (m, 3H), 1.94–1.79 (m, 2H), 1.32 (t, *J* = 7.2 Hz, 3H), 1.29–1.24 (m, 1H), 0.77 (t, *J* = 7.5 Hz, 6H), 0.65–0.56 (m, 2 H) 0.44–0.36 (m, 2H). MS (ESI): 405.5 [MH⁺].

Functional Adenylylase Assay. CHO cells expressing human CB1 or CB2 receptors were seeded 1 day prior to the experiment in DMEM (Invitrogen no. 31331), 1× HT supplement, with 10% fetal calf serum and incubated at 5% CO₂ and 37 °C in a humidified incubator. The growth medium was exchanged with Krebs Ringer bicarbonate buffer with 1 mM IBMX and incubated at 30 °C for 30 min. Compounds to test were added to a final assay volume of 100 μL and incubated for 30 min at 30 °C. By use of the cAMP-Nano-TRF detection kit (Roche Diagnostics), the assay was stopped by the addition of 50 μL of lysis reagent (Tris, NaCl, 1.5% Triton X100, 2.5% NP40, 10% NaN₃) and 50 μL of detection solutions (20 μM mAb Alexa700-cAMP 1:1, and 48 μM ruthenium-2-AHA-cAMP) and shaken for 2 h at rt. The time-resolved energy transfer is measured by a TRF reader (Evotec Technologies GmbH), equipped with a ND:YAG laser as excitation source. The plate is measured twice with

the excitation at 355 nm and at the emission with a delay of 100 ns and a gate of 100 ns, total exposure time of 10 s at 730 nm (bandwidth 30 nm) or 645 nm (bandwidth 75 nm), respectively. The FRET signal is calculated as follows: FRET = T730 – Alexa730 – P(T645 – B645) with $P = (Ru730 - B730)/(Ru645 - B645)$, where T730 is the test well measured at 730 nM, T645 is the test well measured at 645 nm, B730 and B645 are the buffer controls at 730 and 645 nm, respectively. cAMP content is determined from the function of a standard curve spanning from 10 μM to 0.13 nM cAMP. EC₅₀ values were determined using Activity Base analysis (ID Business Solution, Limited). The EC₅₀ values for a wide range of cannabinoid agonists or inverse agonists generated from this assay for reference compounds were in agreement with the values published in the scientific literature.

Radioligand Binding Assay. The binding affinity was determined using membrane preparations from CHO cells expressing the human CB1 or CB2 or murine CB2 receptor in conjunction with [³H]CP-55,940 (PerkinElmer) as radioligand. Binding was performed in binding buffer (50 mM Tris, 5 mM MgCl₂, 2.5 mM EDTA, and 0.5% fatty acid free BSA, pH 7.4, for CB1 receptor and 50 mM Tris, 5 mM MgCl₂, 2.5 mM EGTA, and 0.1% fatty acid free BSA, pH 7.4 for CB2 receptor) in a total volume of 0.2 mL for 1 h at 30 °C shaking. The reaction was terminated by rapid filtration through microfiltration plates coated with 0.5% polyethylenimine (UniFilter GF/B filter plate; Packard). Bound radioactivity was analyzed for K_i using nonlinear regression analysis (Activity Base, ID Business Solution, Limited), with the K_d values for [³H]CP55,940 determined from saturation experiments.³¹

Radiochemistry. [¹⁴C]CO₂ was produced via the ¹⁴N(p,α)¹⁴C nuclear reaction by bombardment of a nitrogen gas target fortified with 0.5% oxygen using a Cyclone 18/9 cyclotron (18 MeV; IBA, Belgium). After reduction over a supported nickel catalyst to [¹⁴C]CH₄ and subsequent gas phase iodination, [¹⁴C]CH₃I was bubbled through a mixture of hydroxyl precursor **15** (0.7 mg) and sodium hydride (1 mg/mL in DMF, 0.4 mL) in DMF (0.2 mL). The mixture was heated to 90 °C for 3 min. After dilution with water (1.4 mL), the crude product was purified using semipreparative HPLC. The collected product was diluted with water (10 mL), trapped on a C18 cartridge (Waters, preconditioned with 5 mL of EtOH and 10 mL of water), washed with water (5 mL), and eluted with EtOH (0.5 mL). For formulation of the final product **16**, saline (9.5 mL) was added to give an ethanol concentration of 5%. For quality control, an aliquot of the formulated solution was injected into an analytical HPLC system. The product was confirmed by co-injection of cold reference compound **6a**. Specific activity of the radiolabeled product was calculated by comparison of UV peak intensity with a calibration curve of the cold reference compound.

Determination of log D_{7.4}. The partition coefficient *D* was determined by the shake-flask method as previously reported.³⁴ In brief, *n*-octanol saturated with phosphate buffer, pH 7.4 (0.5 mL), and phosphate buffer saturated with *n*-octanol (0.5 mL) were mixed with formulated **16** (20 μL, 8 MBq). The samples were shaken for 15 min and centrifuged at 5000g for 5 min. Radioactivity concentrations of both phases were measured in a γ counter (Wizard, PerkinElmer) and *D* was calculated as their ratio.

In Vitro Autoradiography. Mouse and rat spleen tissue were embedded in TissueTek and cut into 20 μm thick sections on a cryostat. The slices were absorbed on SuperFrost Plus slides (Menzel) and stored at –80 °C until use. For the experiment, the slices were thawed on ice for 10 min before conditioning in incubation buffer (50 mM Tris/HCl, 5% BSA, pH 7.4) on ice for 10 min. Excess solution was carefully removed, and the tissue slices were dried for 10 min. The slices were then dripped with 600 μL of incubation buffer containing 0.2 nM **16** and incubated for 15 min at rt in a humid chamber. For blockade conditions, the slices were dripped with 600 μL of a mixture of radioligand (0.2 nM) and **17** (5 μM). After incubation, the slices were washed with washing buffer (50 mM Tris/HCl, 1% BSA, 5% EtOH, pH 7.4) for 2 min (2×) and distilled water for 5 s (2×) on ice. After drying, the slices were exposed (30 min) to appropriate phosphor imager plates (Fuji) and the films were scanned in a BAS5000 reader (Fuji).

In Vitro Stability. Mouse, rat, and human plasma (400 μ L) were incubated with **16** formulated solution (10 μ L, 4 MBq) at 37 °C under shaking. At 5, 10, 15, and 20 min, aliquots (100 μ L) were collected and the reaction was stopped with 100 μ L of ice-cooled CH₃CN. The samples were centrifuged (3 min, 5000 rpm), and the supernatant was collected and analyzed by radio-TLC Instant Imager (Packard, Canberra Company) using hexane/EtOAc (1:1).

In Vivo Metabolic Stability. In vivo stability was performed in a healthy Wistar rat. Radiotracer solution (48 MBq, 0.19 nmol) was injected via tail vein, and blood was collected at 5, 10, and 20 min. After 20 min the rat was sacrificed, urine was collected, and brain was removed. Plasma was separated from the blood cells by centrifugation at 5000g for 5 min at 4 °C. Proteins of plasma and urine were precipitated with ice-cold CH₃CN and then separated by centrifugation. The brain tissue was homogenized in PBS (2 mL), and cold CH₃CN was added to precipitate proteins followed by centrifugation. Supernatants were analyzed by radio-TLC using hexane/EtOAc (1:1). Results are expressed as percentage of total activity.

Biodistribution Studies. For biodistribution studies in male Wistar rats, an amount of 6–10 MBq (0.03–0.05 nmol) of radiotracer solution was administered via tail vein injection into Wistar rats ($n = 3$). For blocking conditions, **17** (1.5 mg/kg) was injected iv shortly before the tracer ($n = 3$). Animals were sacrificed under anesthesia with isoflurane by decapitation at 15 min pi. Blood and organs were collected, weighed, and radioactivity was measured in a γ -counter. The accumulated radioactivity in the organs was expressed as percent normalized injected dose per gram of tissue normalized to 1 kg body weight of the animals (norm. % ID/g tissue). One of the control animals was excluded from data analysis because the tracer was injected paravenously, resulting in low counts in all tissues.

In Vivo PET. For spleen-PET scans, four rats (two baseline and two displacement) were anesthetized with isoflurane, and **16** (11–18 MBq, 0.06–0.09 nmol) was injected via the tail vein. For displacement experiments, 1.5 mg/kg **17** was iv injected 10 min after radiotracer administration. For brain PET scans, eight mice in total (six with LPS treatment) were anesthetized with isoflurane and an amount of 10–27 MBq (0.05–0.014 nmol) **16** was injected via the tail vein. For blocking conditions, 2.0 mg/kg **17** or vehicle was injected sc 30 min before tracer application (two mice each). Two mice were injected sc with 2 mg/kg **17** 10 min before tracer application to evaluate the best protocol for maximal blocking. However, one of the two mice died during the scan.

In both species, PET acquisition was started simultaneously with radiotracer injection and lasted for 60 min followed by CT. Depth of anesthesia of rats or mice was monitored by measuring respiratory frequency (SA Instruments, Inc., Stony Brook, USA). Body temperature was controlled by a rectal probe connected to a thermocoupler for regulating temperature to 37 °C via an air stream. Data were reconstructed in user-defined time frames with a voxel size of $0.3875 \times 0.3875 \times 0.775$ mm³ by two-dimensional-ordered subsets expectation maximization (2D-OSEM). Random and single but no attenuation correction was applied. PET acquisitions were followed by a CT for anatomical orientation. Image files were analyzed with PMOD 3.5 software (PMOD Technologies Ltd., Zurich, Switzerland). Brain regions of interest (ROI) were defined on the mouse MRI T2 template. Tissue radioactivity of the brain ROI was expressed as SUV, that is, the decay-corrected radioactivity per cm³ divided by the injected radioactivity dose per gram of body weight.

■ ASSOCIATED CONTENT

● Supporting Information

Molecular formula strings in csv file. The Supporting Information is available free of charge on the ACS Publications website at DOI: 10.1021/acs.jmedchem.5b00283.

■ AUTHOR INFORMATION

Corresponding Authors

*U.G.: phone, 0041 61 688 54 46; e-mail, uwe.grether@roche.com.

*S.M.A.: phone, 0041 44 6337463; e-mail, simon.ametamey@pharma.ethz.ch.

Notes

The authors declare no competing financial interest.

■ ACKNOWLEDGMENTS

We thank Ernst Schaffter, Anja Osterwald, Elisabeth Zirwes, and Isabella Erbsmehl for their technical assistance and Mark Rogers-Evans and Thomas Hartung for discussions. We thank Bruno Mancosu for his support with carbon-11 module and Claudia Keller for performing PET/CT scans. We thank the Swiss ALS Foundation for partly financing this project and Prof. M. Weber for discussions.

■ ABBREVIATIONS USED

DMTMM, 4-(4,6-dimethoxy-1,3,5-triazin-2-yl)-4-methylmorpholinium chloride; hCB2, human cannabinoid 2 receptor; mCB2, murine cannabinoid receptor type 2; OSEM, ordered subset expectation maximization; PET, positron emission tomography

■ REFERENCES

- (1) Pertwee, R. G.; Howlett, A. C.; Abood, M. E.; Alexander, S. P.; Di Marzo, V.; Elphick, M. R.; Greasley, P. J.; Hansen, H. S.; Kunos, G.; Mackie, K.; Mechoulam, R.; Ross, R. A. International Union of Basic and Clinical Pharmacology. LXXIX. Cannabinoid receptors and their ligands: beyond CB(1) and CB(2). *Pharmacol. Rev.* **2010**, *62*, 588–631.
- (2) Matsuda, L. A.; Lolait, S. J.; Brownstein, M. J.; Young, A. C.; Bonner, T. I. Structure of a cannabinoid receptor and functional expression of the cloned cDNA. *Nature* **1990**, *346*, 561–564.
- (3) Munro, S.; Thomas, K. L.; Abu-Shaar, M. Molecular characterization of a peripheral receptor for cannabinoids. *Nature* **1993**, *365*, 61–65.
- (4) Johns, D. G.; Behm, D. J.; Walker, D. J.; Ao, Z.; Shapland, E. M.; Daniels, D. A.; Riddick, M.; Dowell, S.; Staton, P. C.; Green, P.; Shabon, U.; Bao, W.; Aiyar, N.; Yue, T. L.; Brown, A. J.; Morrison, A. D.; Douglas, S. A. The novel endocannabinoid receptor GPR55 is activated by atypical cannabinoids but does not mediate their vasodilator effects. *Br. J. Pharmacol.* **2007**, *152*, 825–831.
- (5) Overton, H. A.; Fyfe, M. C.; Reynet, C. GPR119, a novel G protein-coupled receptor target for the treatment of type 2 diabetes and obesity. *Br. J. Pharmacol.* **2008**, *153* (Suppl. 1), 76–81.
- (6) McHugh, D.; Hu, S. S.; Rimmerman, N.; Juknat, A.; Vogel, Z.; Walker, J. M.; Bradshaw, H. B. N-Arachidonoyl glycine, an abundant endogenous lipid, potently drives directed cellular migration through GPR18, the putative abnormal cannabidiol receptor. *BMC Neurosci.* **2010**, *11*, 44.
- (7) Szallasi, A.; Di Marzo, V. New perspectives on enigmatic vanilloid receptors. *Trends Neurosci.* **2000**, *23*, 491–497.
- (8) Pertwee, R. G. Pharmacology of cannabinoid CB1 and CB2 receptors. *Pharmacol. Ther.* **1997**, *74*, 129–180.
- (9) Miller, A. M.; Stella, N. CB2 receptor-mediated migration of immune cells: It can go either way. *Br. J. Pharmacol.* **2008**, *153*, 299–308.
- (10) Van Sickle, M. D.; Duncan, M.; Kingsley, P. J.; Mouihate, A.; Urbani, P.; Mackie, K.; Stella, N.; Makriyannis, A.; Piomelli, D.; Davison, J. S.; Marnett, L. J.; Di Marzo, V.; Pittman, Q. J.; Patel, K. D.; Sharkey, K. A. Identification and functional characterization of brainstem cannabinoid CB2 receptors. *Science* **2005**, *310*, 329–332.

- (11) Ashton, J. C.; Friberg, D.; Darlington, C. L.; Smith, P. F. Expression of the cannabinoid CB2 receptor in the rat cerebellum: an immunohistochemical study. *Neurosci. Lett.* **2006**, *396*, 113–116.
- (12) Brusco, A.; Tagliaferro, P.; Saez, T.; Onaivi, E. S. Postsynaptic localization of CB2 cannabinoid receptors in the rat hippocampus. *Synapse* **2008**, *62*, 944–949.
- (13) Benito, C.; Tolon, R. M.; Pazos, M. R.; Nunez, E.; Castillo, A. L.; Romero, J. Cannabinoid CB2 receptors in human brain inflammation. *Br. J. Pharmacol.* **2008**, *153*, 277–285.
- (14) Onaivi, E. S. Cannabinoid receptors in brain: pharmacogenetics, neuropharmacology, neurotoxicology, and potential therapeutic applications. *Int. Rev. Neurobiol.* **2009**, *88*, 335–369.
- (15) Shoemaker, J. L.; Seely, K. A.; Reed, R. L.; Crow, J. P.; Prather, P. L. The CB2 cannabinoid agonist AM-1241 prolongs survival in a transgenic mouse model of amyotrophic lateral sclerosis when initiated at symptom onset. *J. Neurochem.* **2007**, *101*, 87–98.
- (16) Yiangou, Y.; Facer, P.; Durrenberger, P.; Chessell, I. P.; Naylor, A.; Bountra, C.; Banati, R. R.; Anand, P. COX-2, CB2 and P2X7-immunoreactivities are increased in activated microglial cells/macrophages of multiple sclerosis and amyotrophic lateral sclerosis spinal cord. *BMC Neurol.* **2006**, *6*, 12.
- (17) Evens, N.; Muccioli, G. G.; Houbrechts, N.; Lambert, D. M.; Verbruggen, A. M.; Van Laere, K.; Bormans, G. M. Synthesis and biological evaluation of carbon-11- and fluorine-18-labeled 2-oxoquinoline derivatives for type 2 cannabinoid receptor positron emission tomography imaging. *Nucl. Med. Biol.* **2009**, *36*, 455–465.
- (18) Slavik, R.; Bieri, D.; Cermak, S.; Muller, A.; Kramer, S. D.; Weber, M.; Schibli, R.; Ametamey, S. M.; Mu, L. Development and evaluation of novel PET tracers for imaging cannabinoid receptor type 2 in brain. *Chimia (Aarau)* **2014**, *68*, 208–210.
- (19) Horti, A. G.; Gao, Y.; Ravert, H. T.; Finley, P.; Valentine, H.; Wong, D. F.; Endres, C. J.; Savonenko, A. V.; Dannals, R. F. Synthesis and biodistribution of [¹¹C]A-836339, a new potential radioligand for PET imaging of cannabinoid type 2 receptors (CB2). *Bioorg. Med. Chem.* **2010**, *18*, 5202–5207.
- (20) Evens, N.; Vandeputte, C.; Muccioli, G. G.; Lambert, D. M.; Baekelandt, V.; Verbruggen, A. M.; Debyser, Z.; Van Laere, K.; Bormans, G. M. Synthesis, in vitro and in vivo evaluation of fluorine-18 labelled FE-GW405833 as a PET tracer for type 2 cannabinoid receptor imaging. *Bioorg. Med. Chem.* **2011**, *19*, 4499–4505.
- (21) Vandeputte, C.; Evens, N.; Toelen, J.; Deroose, C. M.; Bosier, B.; Ibrahim, A.; Van der Perren, A.; Gijsbers, R.; Janssen, P.; Lambert, D. M.; Verbruggen, A.; Debyser, Z.; Bormans, G.; Baekelandt, V.; Van Laere, K. A PET brain reporter gene system based on type 2 cannabinoid receptors. *J. Nucl. Med.* **2011**, *52*, 1102–1109.
- (22) Ruhl, T.; Deuther-Conrad, W.; Fischer, S.; Gunther, R.; Hennig, L.; Krautscheid, H.; Brust, P. Cannabinoid receptor type 2 (CB2)-selective *N*-aryl-oxadiazolyl-propionamides: synthesis, radiolabelling, molecular modelling and biological evaluation. *Org. Med. Chem. Lett.* **2012**, *2*, 32.
- (23) Hortala, L.; Arnaud, J.; Roux, P.; Oustric, D.; Boulu, L.; Oury-Donat, F.; Avenet, P.; Rooney, T.; Alagille, D.; Barret, O.; Tamagnan, G.; Barth, F. Synthesis and preliminary evaluation of a new fluorine-18 labelled triazine derivative for PET imaging of cannabinoid CB2 receptor. *Bioorg. Med. Chem. Lett.* **2014**, *24*, 283–287.
- (24) Evens, N.; Bosier, B.; Lavey, B. J.; Kozlowski, J. A.; Vermaelen, P.; Baudemprez, L.; Busson, R.; Lambert, D. M.; Van Laere, K.; Verbruggen, A. M.; Bormans, G. M. Labelling and biological evaluation of [(11)C]methoxy-Sch225336: a radioligand for the cannabinoid-type 2 receptor. *Nucl. Med. Biol.* **2008**, *35*, 793–800.
- (25) Ullmer, C.; Zoffmann, S.; Bohrmann, B.; Matile, H.; Lindemann, L.; Flor, P.; Malherbe, P. Functional monoclonal antibody acts as a biased agonist by inducing internalization of metabotropic glutamate receptor 7. *Br. J. Pharmacol.* **2012**, *167*, 1448–1466.
- (26) Pajouhesh, H.; Lenz, G. R. Medicinal chemical properties of successful central nervous system drugs. *NeuroRx* **2005**, *2*, 541–553.
- (27) Galiegue, S.; Mary, S.; Marchand, J.; Dussossoy, D.; Carriere, D.; Carayon, P.; Bouaboula, M.; Shire, D.; Le Fur, G.; Casellas, P. Expression of central and peripheral cannabinoid receptors in human immune tissues and leukocyte subpopulations. *Eur. J. Biochem.* **1995**, *232*, 54–61.
- (28) Gallant, M.; Dufresne, C.; Gareau, Y.; Guay, D.; Leblanc, Y.; Prasit, P.; Rochette, C.; Sawyer, N.; Slipetz, D. M.; Tremblay, N.; Metters, K. M.; Labelle, M. New class of potent ligands for the human peripheral cannabinoid receptor. *Bioorg. Med. Chem. Lett.* **1996**, *6*, 2263–2268.
- (29) Qin, L.; Wu, X.; Block, M. L.; Liu, Y.; Breese, G. R.; Hong, J. S.; Knapp, D. J.; Crews, F. T. Systemic LPS causes chronic neuroinflammation and progressive neurodegeneration. *Glia* **2007**, *55*, 453–462.
- (30) Slavik, R.; Herde, A. M.; Bieri, D.; Weber, M.; Schibli, R.; Krämer, S. D.; Ametamey, S. M.; Mu, L. Synthesis, radiolabeling and evaluation of novel 4-oxo-quinoline derivatives as PET tracers for imaging cannabinoid type 2 receptor. *Eur. J. Med. Chem.* **2015**, *95*, 554–564.
- (31) Bissantz, C.; Grether, U.; Hebeisen, P.; Kimbara, A.; Liu, Q.; Nettekoven, M.; Prunotto, M.; Roever, S.; Rogers-Evans, M.; Schulz-Gasch, T.; Ullmer, C.; Wang, Z.; Yang, W. Pyridine-2-amides useful as CB2 agonists. Patent WO2012168350 A1, 2012.
- (32) Zhou, T.; Zhao, L.; Zhan, R.; He, Q.; Tong, Y.; Tian, X.; Wang, H.; Zhang, T.; Fu, Y.; Sun, Y.; Xu, F.; Guo, X.; Fan, D.; Han, H.; Chui, D. Blood-brain barrier dysfunction in mice induced by lipopolysaccharide is attenuated by dapsone. *Biochem. Biophys. Res. Commun.* **2014**, *453*, 419–424.
- (33) Valenzano, K. J.; Tafesse, L.; Lee, G.; Harrison, J. E.; Boulet, J. M.; Gottshall, S. L.; Mark, L.; Pearson, M. S.; Miller, W.; Shan, S.; Rabadi, L.; Rotshteyn, Y.; Chaffer, S. M.; Turchin, P. I.; Elsemore, D. A.; Toth, M.; Koetzner, L.; Whiteside, G. T. Pharmacological and pharmacokinetic characterization of the cannabinoid receptor 2 agonist, GW405833, utilizing rodent models of acute and chronic pain, anxiety, ataxia and catalepsy. *Neuropharmacology* **2005**, *48*, 658–672.
- (34) Wilson, A. A.; Jin, L.; Garcia, A.; DaSilva, J. N.; Houle, S. An admonition when measuring the lipophilicity of radiotracers using counting techniques. *Appl. Radiat. Isot.* **2001**, *54*, 203–208.